JOURNAL OF GEOPHYSICAL RESEARCH, VOL. 114, F02021, doi:10.1029/2008JF001125, 2009

Improving simulated soil temperatures and soil freeze/thaw at high-latitude regions in the Simple Biosphere/Carnegie-Ames-Stanford Approach model

Kevin Schaefer,[1] Tingjun Zhang,[1] Andrew G. Slater,[1] Lixin Lu,[2,3] Andrew Etringer,[1] and Ian Baker[3]

Received 25 July 2008; revised 17 January 2009; accepted 20 March 2009; published 20 June 2009.

[1] Proper simulation of soil temperature and permafrost at high latitudes in land surface models requires proper simulation of the processes that control snowpack development. The Simple Biosphere/Carnegie-Ames-Stanford Approach (SiBCASA) did not account for depth hoar development and wind compaction, which dominate snow processes at high latitudes. Consequently, SiBCASA had difficulty properly simulating seasonal soil freeze/thaw and permafrost. We improved simulated soil temperatures at high latitudes by (1) incorporating a snow classification scheme that includes depth hoar development and wind compaction, (2) including the effects of organic matter on soil physical properties, and (3) increasing the soil column depth. We ran test simulations at eddy covariance flux tower sites using the North American Regional Reanalysis (NARR) as input meteorology. The NARR captured the observed variability in air temperature, but tended to overestimate precipitation. These changes produced modest improvements in simulated soil temperature at the midlatitude sites because the original snow model already included the weight compaction, thermal aging, and melting processes that dominate snowpack evolution at these locations. We saw significant improvement in simulated soil temperatures and active layer depth at the high-latitude tundra and boreal forest sites. Adding snow classifications had the biggest effect on simulated soil temperatures at the tundra site while the organic soil properties had the biggest effect at the boreal forest site. Implementing snow classes, a deeper soil column, or organic soil properties separately was not sufficient to produce realistic soil temperatures and freeze/thaw processes at high latitudes. Only the combined effects of simultaneously implementing all three changes significantly improved the simulated soil temperatures and active layer depth at the tundra and boreal sites.

Citation: Schaefer, K., T. Zhang, A. G. Slater, L. Lu, A. Etringer, and I. Baker (2009), Improving simulated soil temperatures and soil freeze/thaw at high-latitude regions in the Simple Biosphere/Carnegie-Ames-Stanford Approach model, *J. Geophys. Res.*, *114*, F02021, doi:10.1029/2008JF001125.

1. Introduction

[2] Arctic climate is changing, with air and soil temperatures increasing [*Berner et al.*, 2005; *Intergovernmental Panel on Climate Change*, 2007], permafrost warming [*Osterkamp*, 2007], active layer thickening [*Frauenfeld et al.*, 2004; *Jorgenson et al.*, 2001; *Zhang et al.*, 2005], sea ice declining [*Stroeve et al.*, 2007], and glaciers melting [*Su and Shi*, 2002; *Yao et al.*, 2007]. In Arctic regions, soil temperature, moisture, and freeze-thaw dynamics depend on the physical properties of the soil and snow [*Brown et al.*, 2000; *Zhang et al.*, 2005]. Soil physical properties depend on the amount of organic matter, which is less dense and more porous than pure mineral soil [*Williams and Smith*, 1989]. The insulating effect of snow results in soil temperatures several degrees warmer than annual mean air temperatures and as much as 20° warmer than winter air temperatures [*Zhang*, 2005]. The strength of this insulating effect depends on the timing, duration, depth, grain size, density, and structure of seasonal snow cover. The timing of snowfall heavily influences soil temperature: earlier and deeper snow cover generally results in warmer soils while shallow snow during midwinter or snow cover persisting well into spring can result in colder soils [*Ling and Zhang*, 2004; *Zhang*, 2005].

[3] In situ observations of snow cover, climate, permafrost, biomass, and many other important variables are generally scarce across the vast Arctic regions, so we depend on climate system models and remote sensing to evaluate the current status and potential changes in Arctic climate. To accurately

[1]National Snow and Ice Data Center, Cooperative Institute for Research in Environmental Sciences, University of Colorado at Boulder, Boulder, Colorado, USA.
[2]Cooperative Institute for Research in Environmental Sciences, University of Colorado at Boulder, Boulder, Colorado, USA.
[3]Department of Atmospheric Science, Colorado State University, Fort Collins, Colorado, USA.

0148-0227/09/2008JF001125$09.00

assess Arctic climate, Land Surface Models (LSMs), which represent the terrestrial surface boundary in climate system models, must accurately reproduce Arctic soil temperature and moisture [*Fuchs et al.*, 1978; *Peters-Lidard et al.*, 1998; *Ling and Zhang*, 2005].

[4] The Simple Biosphere/Carnegie-Ames-Stanford Approach (SiBCASA) LSM [*Schaefer et al.*, 2008] produced reasonable soil temperatures at midlatitudes, but had difficulty in simulating seasonal soil freeze/thaw and permafrost conditions at high northern latitudes. In our initial simulations, we found the soil column was too shallow, the soil too conductive in summer, and the snow too insulating in winter such that simulated permafrost always drifted toward thaw, regardless of assumed initial soil temperatures. The original 3.4 m soil column in SiBCASA was too shallow to account for the thermal stabilization effect of cold, deep soils on the simulated active layer depth [*Alexeev et al.*, 2007; *Delisle*, 2007; *Schaefer et al.*, 2007; *Zhang et al.*, 2008]. The original SiBCASA soil model did not account for the insulating effects of near-surface organic matter, making the soil too conductive in summer. In tundra, the drying of the surface peat layer in summer insulates the soil, limiting the depth of the active layer [*Williams and Smith*, 1989]. Lower thermal conductivity in summer due to soil organic matter results in shallower simulated active layer depths and colder soil temperatures [*Yi et al.*, 2007; *Lawrence et al.*, 2008]. The original SiBCASA snow model assumed that the snow processes that dominate at midlatitudes also control snowpack evolution at high latitudes. The SiBCASA snow model did not account for depth hoar development and wind compaction that dominate snowpack development at high latitudes, resulting in low-density, highly insulating snow. The shallow soil column, no organic soil, and no depth hoar and wind compaction in seasonal snow cover result in simulated permafrost temperatures near freezing and very deep active layers.

[5] We hypothesize that only by addressing all three of these problems can the snow and soil models in SiBCASA properly simulate the soil temperature regime, soil freezing and thawing processes, and permafrost conditions at high latitudes. Prior modeling studies already indicate that the combined effects of organic soils and a deeper soil column are required to simulate realistic soil temperatures and active layer depths in permafrost regions [*Nicolsky et al.*, 2007; *Yi et al.*, 2007]. We hypothesize that the model must also account for the effects of depth hoar development and wind compaction to properly represent the insulating effects of snow. We deepened the SiBCASA soil column to 15 m [*Schaefer et al.*, 2007], incorporated the *Lawrence and Slater* [2008] organic soil model, and incorporated the *Sturm et al.* [1995] snow classification system. We further hypothesize that the *Sturm et al.* [1995] snow class system will account for the effects of depth hoar development and wind compaction on simulated snow density without the expense and complexity of explicitly modeling the processes. For each snow class, we assume generic density stratification on the basis of field observations at thousands of snow course stations across North America. The assumed density stratification changes relative to the simulated snow depth and bulk density, allowing the snowpack to vary with local conditions and with time, but forcing the simulated snow densities to fall within a realistic range of observed values.

[6] Here we describe the changes to SiBCASA to integrate the *Sturm et al.* [1995] snow classes, the *Lawrence and Slater* [2008] organic soil model, and a deeper soil column [*Schaefer et al.*, 2007]. We describe the *Sturm et al.* [1995] snow class system and the snow observations from the North American network of snow course sites and meteorological stations used to determine the vertical snow density profiles. We evaluate model performance by comparing simulated and observed snow density, snow depth, and soil temperatures at selected eddy covariance flux tower sites in the AmeriFlux network selected to represent each class in the *Sturm et al.* [1995] system.

2. Model Description

2.1. SiBCASA Overview

[7] SiBCASA combines the biophysical Simple Biosphere model, version 3.0 (SiB3.0), with the carbon biogeochemistry from the Carnegie-Ames-Stanford Approach (CASA) model [*Schaefer et al.*, 2008; *Sellers et al.*, 1986, 1996a, 1996b; *Denning et al.*, 1996]. SiBCASA computes surface energy and carbon fluxes at 10–20 min time steps for use in atmospheric circulation models. SiBCASA has integrated water, energy, and carbon cycles and predicts as prognostic variables the moisture contents and temperatures of the canopy and soil [*Sellers et al.*, 1996a]. *Vidale and Stöckli* [2005] added canopy air space CO_2 concentration, humidity, and temperature as prognostic variables. Fluxes of latent and sensible heat include the effects of snow cover, rainfall interception by the canopy, and aerodynamic turbulence [*Sellers et al.*, 1996a].

[8] To calculate plant photosynthesis, SiBCASA uses the Ball-Berry stomatal conductance model [*Ball*, 1988] as modified by *Collatz et al.* [1991] coupled to a modified version of the *Farquhar et al.* [1980] C3 enzyme kinetic model and the *Collatz et al.* [1992] C4 photosynthesis model. Leaf photosynthesis is scaled to the canopy level using the absorbed fraction of Photosynthetically Active Radiation (f_{PAR}) derived from the remotely sensed Normalized Difference Vegetation Index (NDVI) [*Sellers et al.*, 1994, 1996a, 1996b]. The prognostic variables in SiBCASA include biomass in live carbon pools (leaves, roots, and wood), surface litter pools, and soil carbon pools. SiBCASA calculates respiration losses due to microbial decay (heterotrophic respiration) and plant growth (autotrophic respiration). The transfers of carbon from pool to pool and associated respiration losses vary with soil temperature and moisture.

2.2. Snow Classes

[9] Five processes affect snow properties: melting, thermal aging, weight compaction, wind compaction, and depth hoar development [*Anderson*, 1976]. Melting is the increase in snow density due to melting and refreezing of snow. Thermal aging realigns molecules in the snow crystals to reduce surface free energy, changing the snow grains to round or oblong crystals and allowing greater compaction and increased density. Weight compaction is compression due to the mass of overlying snow. Wind compaction occurs when saltation of snow particles fractures and rounds the snow grains, allowing greater compaction and increased snow density. Depth hoar development occurs when strong vertical temperature gradients cause water vapor from the base of the snowpack to

Table 1. Snow Classes and North American Area Fractions[a]

Snow Class	Depth Hoar	Melt	Thermal Aging	Wind	Weight	Total Area Fraction (%)	Snow Area Fraction (%)
Tundra	Yes		Yes	Yes		20.0	28.1
Taiga	Yes		Yes		Yes	17.9	25.2
Maritime		Yes	Yes		Yes	13.0	18.3
Ephemeral		Yes				26.8	na
Prairie			Yes	Yes		13.7	19.3
Alpine			Yes		Yes	6.5	9.2

[a]*Sturm et al.* [1995].

diffuse upward and condense at other locations within the snowpack.

[10] Which processes dominate snowpack development depend on local climate conditions (wind, precipitation, and air temperature), which *Sturm et al.* [1995] used to develop a global snow classification system (Table 1). Each snow class is dominated by a different combination of processes, resulting in characteristic density, crystal morphology, grain size, and horizontal stratification. The tundra class consists of thin, cold snow cover with few melt features with a wind slab layer atop a depth hoar layer. The taiga class consists of fairly deep, cold snow with a thick depth hoar layer. The maritime class consists of deep, wet snow with a lot of melt features. The alpine class is a transitional snow cover between taiga and maritime: too warm to be taiga and not deep enough to be maritime. However, the weather patterns alternate between taiga and maritime conditions, resulting in stratification of dissimilar layers and a unique alpine snow class. The prairie class consists of thin, windblown snow not cold enough to form depth hoar. The ephemeral class consists of intermittent, quickly melting snow or regions that never receive snow.

[11] The geographic distribution of snow classes in North America (Figure 1) roughly corresponds to well-known climatic zones: tundra class roughly in the continuous permafrost zone, taiga class in discontinuous permafrost zone and boreal forests, maritime class in temperate forests, and prairie class in temperate grasslands. The alpine class is concentrated in mountainous regions, but also occurs as a transition between maritime and taiga classes. The ephemeral class straddles the southern limit of seasonal snow cover and includes regions that never receive snow. Snow classes dominated by depth hoar development and wind compaction (tundra, taiga, and prairie) collectively cover half of North America and nearly 2/3 of regions with seasonal snow cover (excluding ephemeral snow).

2.3. Snow Model

[12] SiBCASA uses a snow model derived from the Community Land Model in the Community Climate System Model, Version 3.0 [*Dai et al.*, 2003; *Oleson et al.*, 2000]. The snow model has a variable number of snow layers up to a maximum of five, depending on snowfall amount and history (Figure 2). The thickness of each snow layer increases geometrically with depth from the top of the snowpack. To maintain stability in snow temperature calculations, layer thickness is held nearly constant within a narrow range, except the fifth layer, which, if it exists, has no maximum thickness limit. When layer thickness exceeds a maximum value during a snow event, mass is transferred to the layer below, with new layers forming on the bottom of the snowpack. When layer thickness falls below a minimum value during aging, compression, and melting, mass is transferred up from below, with bottom layers disappearing first.

[13] The prognostic variables for the snow model are temperature for each layer, total snow depth (D) and total snow mass (M_t). The snow density per layer varies with time in response to various compaction processes and SiBCASA transfers mass between layers to maintain constant layer thickness. With mass freely redistributed within the snow column to maintain constant layer thickness, mass per layer is a diagnostic, rather than a prognostic, variable.

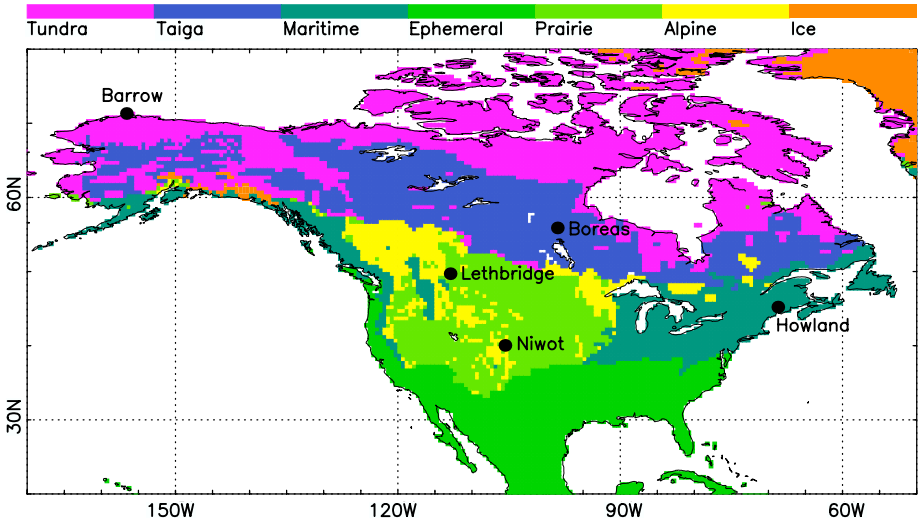

Figure 1. Map of *Sturm et al.* [1995] snow classes for North America and the eddy covariance flux tower sites selected for model evaluation.

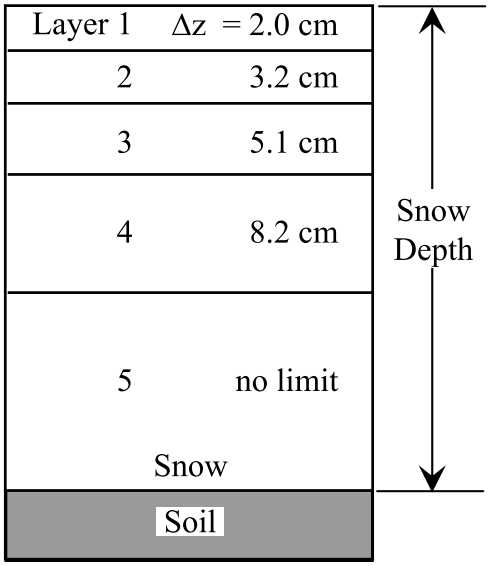

Figure 2. The SiBCASA snow model has a variable number of snow layers. The thickness of each layer increases with depth but is constant in time. New layers are formed or lost on the bottom as snow depth changes over time.

[14] SiBCASA separately tracks ice and water in each layer, but liquid water, when present, cannot exceed 3.3% of the pore space in any layer. Excess water drains down through the snow to eventually infiltrate the soil or contribute to runoff. The original snow model drained excess water such that a layer lost mass, but not thickness. As a result, bulk snow density (ρ_{bulk}) decreased during spring melt, exactly opposite of what is observed. To correct this, we decreased layer thickness proportional to the volume of water that drains out.

[15] Snow depth in the snow model decreases with time, accounting for thermal aging, weight compaction, and melting based on *Anderson* [1976]. The original snow model did not include depth hoar development and wind compaction, primarily because of computational limits. Simulating depth hoar requires representation of water vapor diffusion within the snowpack and simulating wind compaction requires representation of subgrid, horizontal transport of snow, both of which are very difficult to model and computationally expensive.

[16] To approximate the effects of depth hoar development and wind compaction, we superimpose a two-layer vertical density profile over the five-layer mass model (Figure 3) and make special calculations for the depth hoar and wind slab layers in the tundra, taiga, and prairie snow classes. The vertical density profile represents a generalized stratification resulting from the dominant snow processes in each class at full maturity in late winter before the spring melt. Tundra snow has a dense wind slab layer atop a depth hoar layer [*Sturm et al.*, 1995; *Zhang et al.*, 1996; *Domine et al.*, 2002; *Sturm et al.*, 2008]. Taiga snow has a depth hoar layer below a layer of medium density snow. Prairie snow has a wind slab layer atop a compaction layer. Maritime, alpine, and ephemeral classes are dominated by compaction processes, so the top layer has increasing density with depth and a uniform density bottom layer [*Sturm et al.*, 1995; *Iida et al.*, 2000].

[17] Two parameters define our two-layer density stratification: the bottom layer fraction (f_{bot}) and the difference in density between the two layers ($\Delta\rho$). f_{bot} varies with D

$$f_{bot} = f_{botmax}/\left(1 + \exp\left(D_{slope}(D_{half} - D)\right)\right), \quad (1)$$

where f_{botmax} is the maximum observed value of f_{bot}. D_{slope} and D_{half} are the f_{bot} slope and half point

$$\begin{aligned} D_{half} &= (D_{max} + D_{min})/2 \\ D_{slope} &= 10/(D_{max} - D_{min}), \end{aligned} \quad (2)$$

where D_{min} is the minimum snow depth where a bottom layer forms and D_{max} is the snow depth where f_{bot} reaches a maximum value. $\Delta\rho$ depends on both D and ρ_{bulk}

$$\begin{aligned} \Delta\rho = \mathrm{abs}\left(\rho_{topref} - \rho_{botref}\right)(f_{bot}/f_{botmax}) \\ \cdot \exp\left(-(\rho_{bulk} - \rho_{bulkobs})^2/\sigma^2_{bulkobs}\right), \end{aligned} \quad (3)$$

where ρ_{topref} and ρ_{botref} are reference densities for the top and bottom layers of the two-layer vertical density profile, and $\rho_{bulkobs}$ and $\sigma_{bulkobs}$ are the mean and standard deviation of observed bulk density. Here ρ_{topref}, ρ_{botref}, $\rho_{bulkobs}$, and $\sigma_{bulkobs}$ correspond to maximum horizontal stratification in the snowpack, which we assume occurs in late winter. At each time step, SiBCASA calculates f_{bot}, $\Delta\rho$, and the required density of each of the layers in the five-layer snow mass model, redistributing ice and water between layers accordingly. Thermal aging, weight compaction, and melting still determine simulated D and ρ_{bulk}, but the distribution of mass between layers reflects observed stratification for each snow class.

[18] The dependence of f_{bot} and $\Delta\rho$ on D and ρ_{bulk} approximates the evolution of horizontal stratification during the winter season and allows local conditions to influence the snowpack development. To illustrate, Figure 4 shows f_{bot} as a function of D and Figure 5 shows $\Delta\rho$ as a function of ρ_{bulk} for the tundra snow class, assuming maximum stratification ($f_{bot} = f_{botmax}$). Generally, ρ_{bulk} increases during the snow season as various processes compact the snow. In fall when the snow is new with minimal stratification, D is small and ρ_{bulk} low, such that $\Delta\rho$ is near zero. In late winter when the snowpack is mature with maximum stratification, D is large and $\rho_{bulk} \sim \rho_{bulkobs}$, such that $\Delta\rho$ is near its maximum possible value. In spring when snow is melting and stratification breaks down, D is small and ρ_{bulk} large, such that $\Delta\rho$ is again near zero. Since D and ρ_{bulk} are prognostic variables, variations in local weather conditions, such as frequent melt events, change the horizontal stratification. We assume maximum stratification occurs when the snowpack is fully mature in late winter, but the actual evolution of the stratification depends on local conditions.

[19] For tundra and taiga snow, we assume constant thermal conductivity for the bottom depth hoar layer to approximate the changes in grain structure that result from water vapor diffusion and deposition. In the original snow model, the estimated snow thermal conductivity increases with density, assuming that higher density increases contact between snow grains, resulting in higher thermal conductivity

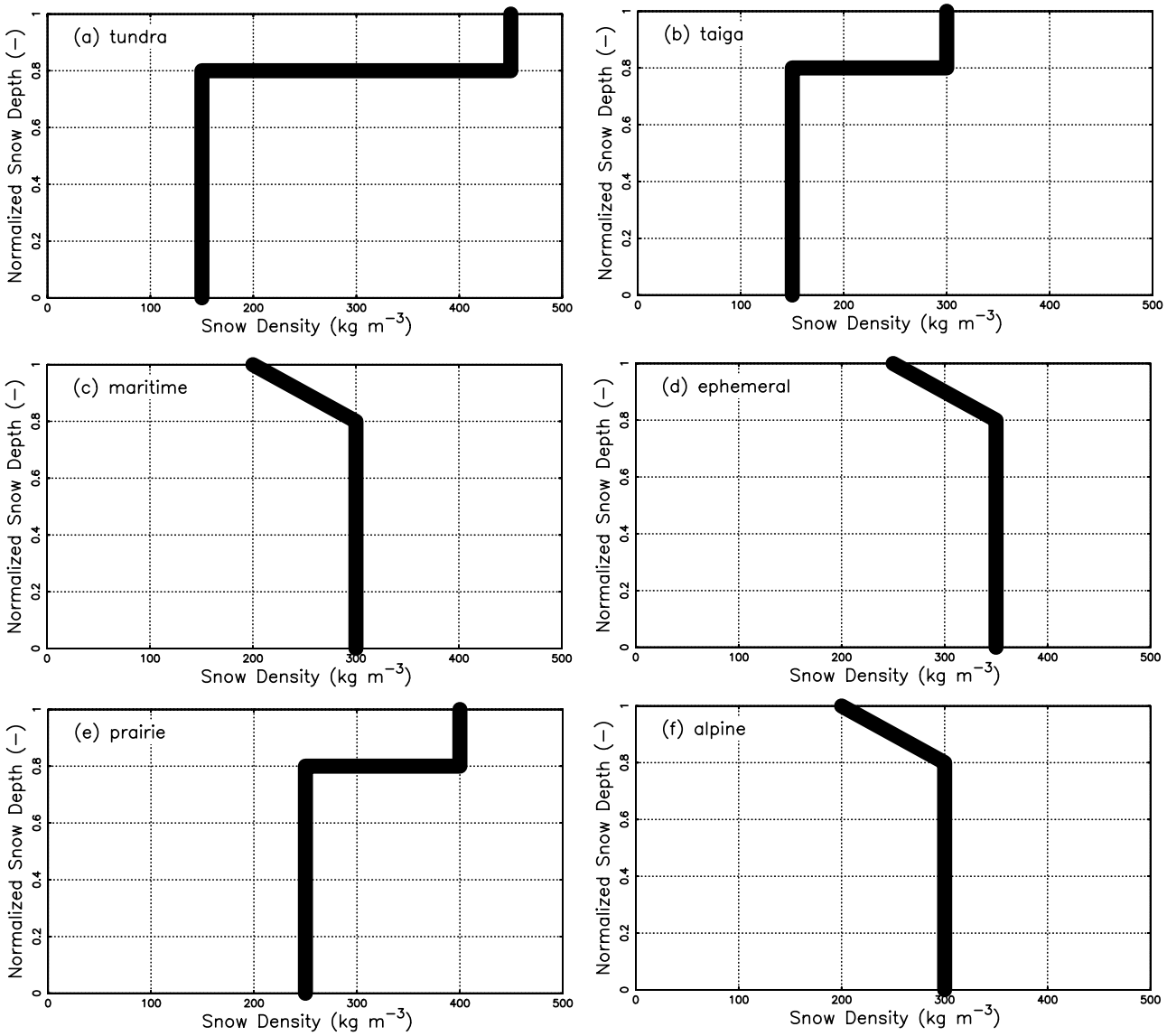

Figure 3. The two-layer snow density model representing maximum horizontal stratification for each snow class.

[*Anderson*, 1976; *Sturm et al.*, 1997]. However, vapor deposition occurring during depth hoar development creates ice bridges between relatively large snow grains, resulting in a low thermal conductivity independent of snow density [*Sturm et al.*, 1997]. For tundra snow, wind slab layers from early winter are eventually buried and transformed into "indurated" or hardened depth hoar [*Sturm et al.*, 2008]. Having started from higher initial density, the indurated depth hoar in tundra snow has a higher thermal conductivity than depth hoar found in taiga snow. On the basis of field observations, we assumed a thermal conductivity of 0.18 W m^{-1} K^{-1} for tundra depth hoar in tundra snow and 0.072 W m^{-1} K^{-1} for taiga depth hoar [*Sturm et al.*, 1997].

[20] For tundra and prairie snow, we approximate wind compaction by increasing the density of new fallen snow with wind speed as well as air temperature

$$\rho_{new} = \rho_{\min} + \delta\rho_T + \delta\rho_w, \tag{4}$$

where ρ_{new} is the density of new fallen snow, $\rho_{\min}$ is the minimum possible new snow density (50 kg m^{-3}), $\delta\rho_T$ is a temperature correction factor, and $\delta\rho_w$ is a wind correction factor. All snow classes include $\delta\rho_T$ based on a curve fit of observed new snowfall densities in mountainous regions at midlatitudes [*Judson and Doesken*, 2000]:

$$\begin{array}{ll} T_{\text{air}} < -15 & \delta\rho_T = 0 \\ T_{\text{air}} \geq = -15 & \delta\rho_T = 1.7(T_{\text{air}} + 15)^{1.5}, \end{array} \tag{5}$$

where T_{air} (°C) is air temperature and 1.7, 15, and 1.5 are empirical constants. In tundra regions, T_{air} is less than −15°C nearly all winter such that in the original model, $\rho_{\text{new}} \sim \rho_{\min}$, producing low-density simulated snowfall, exactly opposite of observed [*Sturm et al.*, 2008]. To correct this, tundra and prairie snow include $\delta\rho_w$ that increases with wind speed, while for all other snow classes, $\delta\rho_w = 0$. $\delta\rho_w$ is based on

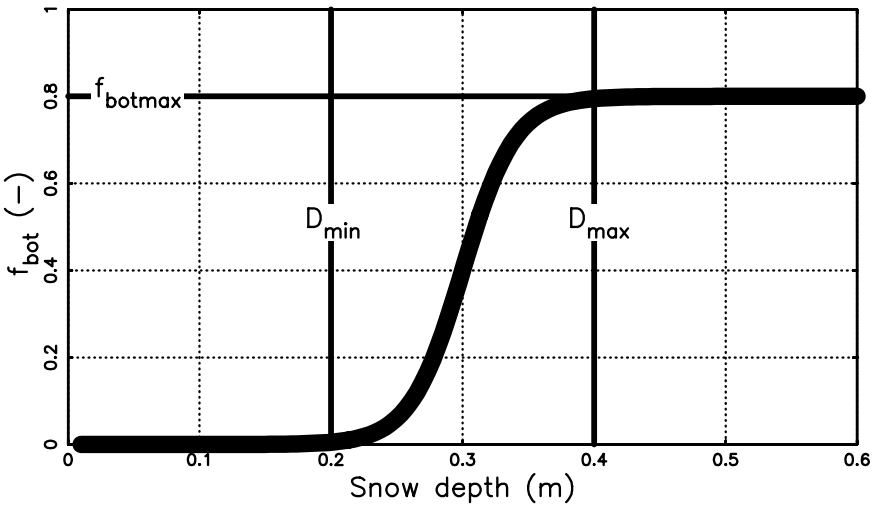

Figure 4. Relative thickness of the bottom layer of the two-layer snow density model (f_{bot}) as a function of snow depth for the tundra snow class. D_{min} is the minimum snow depth where a bottom layer forms and D_{max} is the snow depth where f_{bot} reaches a maximum value, f_{botmax}.

observed grain fracture rates from wind tunnel tests using artificial snow [*Sato et al.*, 2008]

$$\begin{aligned} u < 2 \quad & \delta\rho_w = 0 \\ u \geq 2 \quad & \delta\rho_w = (u-2)\left(\rho_{topref} - \rho_{min}\right)/3, \end{aligned} \tag{6}$$

where u is wind speed (m s^{-1}). Here ρ_{topref} is the maximum observed density of the wind slab layer for the tundra and prairie classes. *Sato et al.* [2008] found that snow grains did not fracture for wind speed less than 2 m s^{-2}, so $\delta\rho_w = 0$ and the fracture rate increased linearly with u > 2 m s^{-1}. We assume maximum ρ_{new} occurs when snow grains are completely decomposed into ice crystals at u between 5 and 6 m s^{-1}. We restrict ρ_{new} to keep it within observed wind slab densities

$$\rho_{new} = \mathrm{MIN}\left(\rho_{new}, \rho_{topref}\right). \tag{7}$$

2.4. Snow Data

[21] Table 2 lists values for the seven time-invariant parameters used to calculate f_{bot}, $\Delta\rho$, and ρ_{new} for each snow class. Here f_{botmax}, D_{min}, D_{max}, ρ_{topref}, and ρ_{botref} represent horizontal stratification within the snowpack. Also, $\rho_{bulkobs}$ and $\sigma_{bulkobs}$ represent observed snow density and density variability at the time of maximum horizontal stratification, which we assume occurs in late winter. The reference month in Table 2 is the assumed month of maximum horizontal stratification. The tundra and taiga classes are generally further north and have later reference months than the other snow classes.

[22] We obtained values for stratification parameters (f_{botmax}, D_{min}, D_{max}, ρ_{topref}, and ρ_{botref}) from the literature. Stratification parameter values for the maritime, ephemeral, and alpine snow classes are based on observations by *Iida et al.* [2000]. Stratification parameter values for tundra and taiga classes are based on observations by *Domine et al.*

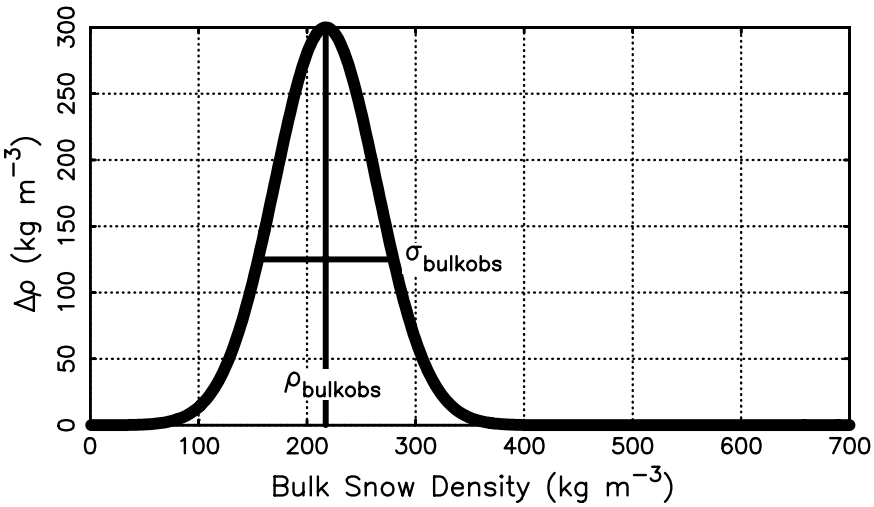

Figure 5. Density difference between top and bottom layers ($\Delta\rho$) as a function of bulk snow density for the tundra snow class, assuming maximum stratification. Here $\rho_{bulkobs}$ and $\sigma_{bulkobs}$ are the mean and standard deviation of observed bulk density for the tundra snow class.

Table 2. Snow Class Parameters

Class	f_{botmax}	D_{min} (m)	D_{max} (m)	ρ_{topref} (kg m^{-3})	ρ_{botref} (kg m^{-3})	ρ_{bulk} (kg m^{-3})	$\rho_{bulkstd}$ (kg m^{-3})	Reference Month
Tundra	0.3	0.0	0.1	350	100	261.108	68.206	April
Taiga	0.7	0.0	0.7	300	200	213.363	49.462	March
Maritime	0.8	0.2	0.8	200	300	286.501	80.979	February
Ephemeral	0.8	0.2	0.8	250	350	321.289	82.321	February
Prairie	0.8	0.2	0.8	350	250	272.423	61.057	February
Alpine	0.8	0.2	0.7	200	300	267.796	56.85	February

[2002]. For the prairie class, we assume the top layer is similar to the wind packed layer of tundra and the bottom layer is similar to maritime snow.

[23] We calculated $\rho_{bulkobs}$ and $\sigma_{bulkobs}$ for each snow class from a statistical analysis of observed snow depth and snow water equivalent (SWE) from 5370 snow course sites across North America [*Brown*, 2000; *Natural Resources Conservation Service*, 2007]. A snow course is a site where manual measurements of snow depth and SWE are taken by trained observers. Generally, the courses are ~300 m long and are situated in small meadows protected from the wind [*Natural Resources Conservation Service*, 2007]. Measurements are usually taken around the first of the month during the winter and spring. Historically, there are 2993 snow course sites in Canada and 2377 in the USA where both snow depth and SWE were measured, although the actual number of sites varies with time. Snow surveys in North America date back to the mid-1900s, while the regional surveys started in the mid-1930s in the western USA and the mid-1950s in Canada.

[24] To calculate $\rho_{bulkobs}$ and $\sigma_{bulkobs}$, we collected available digital snow course data from the beginning of the record at each site through 2006. After careful data quality control, we estimated observed snow bulk density at each site by dividing SWE by snow depth, assuming both were constant under a unit area at the time of measurement. We calculated an arithmetic mean if there were more than one measurement within a month. For each snow course site, we excluded snow-free periods and calculated the long-term mean and standard deviation of the observed snow bulk density for each month of the winter season. We then projected the snow course sites onto the $0.5^\circ \times 0.5^\circ$ snow class map [*Sturm et al.*, 1995; *Liston and Sturm*, 1998] and calculated the monthly mean and standard deviation of the observed snow bulk densities for each snow class, excluding ice (see Figure 8). We then assigned the mean and standard deviation of observed bulk snow density for the reference month to $\rho_{bulkobs}$ and $\sigma_{bulkobs}$ in Table 2.

2.5. Soil Model

[25] SiBCASA uses a soil temperature and hydrology model with explicit treatment of frozen soil water originally from the Community Climate System Model, Version 2.0 [*Bonan*, 1996; *Oleson et al.*, 2000]. The original configuration had 10 soil layers with an exponential increase in layer thickness, from 2 to 127 cm, to a total depth of 3.4 m. However, to properly reproduce the seasonal cycle in soil temperatures, the soil model must be three times the damping depth [*Schaefer et al.*, 2007], where damping depth is the depth at which the amplitude of the seasonal cycle in soil temperature is $1/e$ the surface amplitude. Damping depth ranges between 2 and 3 m for seasonally frozen soil and 3–4 m for permafrost [*Schaefer et al.*, 2007], indicating a required total soil depth between 6 and 9 m. We increased the number of soil layers to 25, with geometrically increasing thickness, from 2 to 280 cm, to a total depth of 15 m.

[26] Following *Lawrence and Slater* [2008], we assume soil physical, hydraulic, and thermodynamic properties are weighted averages between those of pure mineral soil and pure organic soil. For example, the soil porosity, P, is

$$P = (1 - f_o)P_{min} + f_o P_o, \tag{8}$$

where P_{min} is the porosity of pure mineral soil and P_o is the porosity of pure organic soil. The organic soil fraction for a soil layer, f_o, is the ratio of simulated to maximum possible organic mass

$$f_o = (M_o / M_{o\,max}), \tag{9}$$

where M_o is the simulated mass of organic matter for a particular soil layer and M_{omax} is the mass of organic matter for pure organic soil

$$M_{o\,max} = \rho_{o\,max}\Delta z, \tag{10}$$

where ρ_{omax} is the density of pure organic soil and Δz is layer thickness. Calculation of soil porosity, thermal conductivity, heat capacity, saturated hydraulic conductivity, and matrix potential follow *Lawrence and Slater* [2008].

[27] Our only differences from *Lawrence and Slater* [2008] are (1) time-dependent soil carbon content and (2) a different value of ρ_{omax}. *Lawrence and Slater* [2008] assume a ρ_{omax} of 130 kg m^{-3}, but we assume ρ_{omax}, is 140 kg m^{-3} on the basis of more recent observations of bulk densities of peat [*Price et al.*, 2005]. *Lawrence and Slater* [2008] assumed constant soil organic matter content, but we allow M_o to vary with time on the basis of the SiBCASA prognostic carbon pools. In SiBCASA, the soil carbon content of each layer decreases with depth proportional to relative root density, such that

$$M_o = C_{tot} F_{root} r_{carb}, \tag{11}$$

where C_{tot} is the total soil carbon for the entire soil column, f_{root} is the fraction of total roots within that layer, and r_{carb} is the ratio of organic matter to carbon (assumed equal to 2) [*Miller et al.*, 2004]. C_{tot} includes all soil organic matter, fine root biomass, woody root biomass, and belowground coarse woody debris (assumed to be 25% of the wood and coarse woody debris pools [*Jenkins et al.*, 2001]). The topsoil layer includes all surface litter and 75% of coarse woody debris.

2.6. Model Evaluation

[28] To evaluate our changes to the snow and soil models, we compared simulated and observed D, ρ_{bulk}, and soil temperature at five eddy covariance flux tower sites in the

Table 3. Towers Selected for Model Evaluation

Tower	Snow Class	Biome Type	Start	Stop	Reference
Barrow	Tundra	Tundra	1998	2001	*Eugster et al.* [2000]
Boreas Old Black Spruce	Taiga	Boreal Forest	1994	2004	*Dunn et al.* [2007]
Howland Forest	Maritime	Mixed Deciduous	1996	2003	*Hollinger et al.* [2004]
Lethbridge	Prairie	Grassland	1998	2005	
Niwot Ridge Forest	Alpine	Evergreen Forest	1998	2005	*Monson et al.* [2002]

AmeriFlux network (Table 3). Each flux tower site represents a different snow class, excluding ephemeral and ice. Barrow is a tundra site on the north slope of Alaska. Boreas is a mature black spruce forest site from the Boreal Ecosystem-Atmosphere Study (BOREAS). Howland is a mature, mixed needleleaf-deciduous forest in Maine. Lethbridge is a prairie site located on the western edge of the Canadian plains. Niwot is an evergreen forest located on Niwot Ridge in the Rocky Mountains of central Colorado. These flux towers primarily measure surface fluxes of sensible heat, latent heat and carbon [*Baldocchi*, 2003], but also have extensive observations of local weather, biomass, snow depth, and soil temperature. Our SiBCASA evaluation compared simulated and observed soil temperature, snow depth, and, if available, soil biomass.

[29] As input, SiBCASA requires meteorological forcing data, absorbed fraction of Photosynthetically Active Radiation (f_{PAR}), Leaf Area Index (LAI), and soil texture. We estimate f_{PAR} and LAI from the GIMMS NDVI data set, version g [*Tucker et al.*, 2005] using procedures described by *Sellers et al.* [1996b], *Los et al.* [2001], and *Schaefer et al.* [2002, 2005]. GIMMS consists of global, monthly composite maps of NDVI at 8 km resolution. We extract NDVI for each flux tower site and assign biome specific biophysical parameters from *Sellers et al.* [1996b]. We use soil textures from $1^\circ \times 1^\circ$ maps of percent sand, silt, and clay interpolated from the International Global Biosphere Program soil core database.

[30] For meteorological forcing, we extract data for each flux tower site from the North American Regional Reanalysis (NARR) [*Mesinger et al.*, 2006]. Observations at each flux tower site include local weather conditions; however SiBCASA requires continuous data, and filling inevitable gaps in observed weather is somewhat arbitrary and often produces errors. The NARR is internally consistent, reanalyzed weather at 32 km resolution for the North American domain from 1979 to present. NARR assimilates precipitation observations into the atmospheric analyses, improving the simulated hydrological cycle. SiBCASA uses NARR surface temperature, pressure, wind speed, precipitation, and radiation data every three hours. Except for incident light, SiBCASA linearly interpolates NARR weather in time between input data points. We scale incident light by the cosine of the solar zenith angle to conserve incoming energy and assure that no light falls on the canopy at night [*Zhang et al.*, 1996]. To evaluate the effects of errors in meteorological forcing on simulated soil temperatures and snow properties, we compared NARR and observed air temperatures and precipitation.

[31] We ran simulations at each flux tower site from 1982 and 2003 (22 years), when GIMMS and NARR overlapped. To spin up SiBCASA to steady state, we ran three, 22-year simulations (66 years total), repeating the NARR and GIMMS data. For initial values in the first simulation, we assumed soil temperatures equal to the NARR annual mean air temperature, soil moisture at 95% saturation, and all carbon pools equal to 100 mol C m^{-2}. We used time mean decay rate constants from the first simulation to calculate steady state pool sizes to start the second simulation [*Schaefer et al.*, 2008]. Since the pool sizes and soil porosity change, we reinitialized the soil moisture to 95% at the start of the second simulation. Otherwise, soil temperature and other prognostic variables from the end of one simulation are used as initial values for the next. To evaluate what model change most improved simulated soil temperature, we also ran baseline simulations with the original SiBCASA model and a series of simulations including only the deeper soil column, snow classes, or organic soil properties.

[32] At each flux tower site, we compared observed soil temperatures with the simulated soil temperatures extracted from the appropriate model soil layer. At Barrow and Boreas we used separate data sets of observed soil temperatures at multiple depths down to a maximum of 1 m [*Sutton et al.*, 1998; *Hinkel*, 1998]. We evaluated how differences between NARR and observed air temperature and precipitation influenced simulated soil temperatures. We compared simulated and observed organic matter content, snow depth, and snow density. Observed snow depth was not available at the flux tower sites, so we compared simulated snow depths with observed values at the nearest meteorological observing stations (Table 4). Neither the flux tower observations nor the nearest observing stations included observed snow bulk density, so we compared simulated snow bulk density to the average seasonal cycle of observed bulk density for all snow course observations within that class for North America.

3. Results

3.1. NARR Evaluation

[33] The NARR air temperature captured the seasonal and synoptic variability of the observed air temperature at each tower site. Figure 6 shows the NARR and observed air temperature at all sites for the winter of 2002–2003. On the basis of a statistical analysis of the difference between NARR and observed air temperatures, we found that the NARR captured the magnitude of the synoptic variability, but small differences in the timing of synoptic events result in instantaneous differences between 0° and ±10°C at each site. When calculating daily average air temperature, these differences averaged out to ±5°C at all sites except Barrow, which remained at ±10°C.

Table 4. Nearest Observing Station to Each Tower

Tower	Nearest Snow Course	Distance (km)
Barrow	Barrow WSO Airport	6.32
Boreas	Thompson Airport	39.20
Howland	Dover-Foxcroft	40.05
Lethbridge	Lethbride Airport	13.41
Niwot	Niwot Ridge C1	0.96

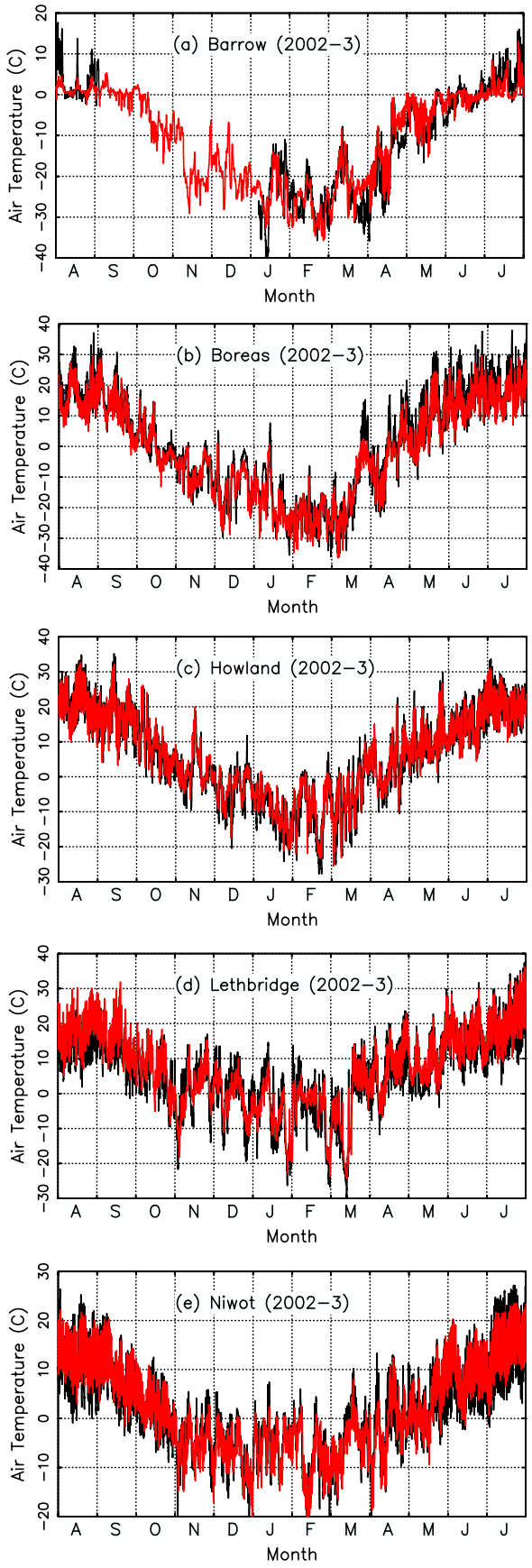

Figure 6. Observed (black) and NARR (red) air temperature at 30-min resolution for all sites during the winter season of 2002–2003.

[34] When averaged to a monthly time scale, some sites show a seasonal bias: NARR temperatures at the Boreas site are 3°C colder than observed in summer while NARR temperatures at the Niwot and Lethbridge sites are 3°C colder than observed in winter. NARR temperatures at the Barrow site are 3°C colder than observed in summer and 4°C warmer than observed in spring and fall. These biases cancel when averaging over a year to less than ±1°C at all sites except Barrow, where the annual biases were ±2°C. Considering all time scales, NARR matched observed temperatures best at the Howland site, followed closely by the Lethbridge and Niwot sites and the worst at the Barrow site.

[35] The NARR tends to overestimate precipitation, although gaps in observed precipitation make it difficult to quantify by how much. The timing of specific precipitation events often did not coincide with locally observed precipitation because NARR is not perfectly synchronized to observed synoptic variability. Consequently, we compared only monthly and annual total NARR and observed precipitation. Figure 7 shows the total monthly precipitation at each site for the winter of 2002–2003, except the Lethbridge site, where we only had observed precipitation data for 2006. For the monthly precipitation totals, we included only those NARR values with a corresponding valid observation.

[36] Comparisons at the Barrow and Boreas sites are ambiguous because 50% of the observations were missing at each site and most of the missing data occurred in winter. Each site shows little or no observed precipitation during winter, which seems unrealistic. Using a different data set, *Zhang et al.* [1996] estimate an annual total precipitation at the Barrow site of ~175 mm while NARR shows an annual total precipitation of ~300 mm. At the Barrow and Boreas sites, NARR clearly overestimates precipitation by at least a factor of two. At the Howland site, NARR consistently overestimated precipitation all year. At the Lethbridge site, NARR matched observed precipitation in summer, but overestimated precipitation in winter. At the Niwot site, NARR precipitation agreed with observed values all year. Overall, NARR precipitation matches observed precipitation at the Niwot site, but overestimates precipitation at all other sites.

3.2. Snow Density

[37] Simulated bulk snow density for all sites increases with time within the variability of observed bulk density (Figure 8). The black lines are the average seasonal cycle for all snow course observations within that class for North America and the gray bars represent the standard deviation of observed bulk snow density, which we interpret as a measure of uncertainty. The red lines are the average seasonal cycle of monthly average, simulated snow bulk density (with snow-free periods removed). Barrow shows an overall positive bias, but falls outside the range of observed variability only in February and March. The tundra snow class shows a midwinter decline in observed bulk density that our simplified representations of depth hoar development and wind compaction do not capture. The Boreas and Howland sites show the best match with observations, although Boreas

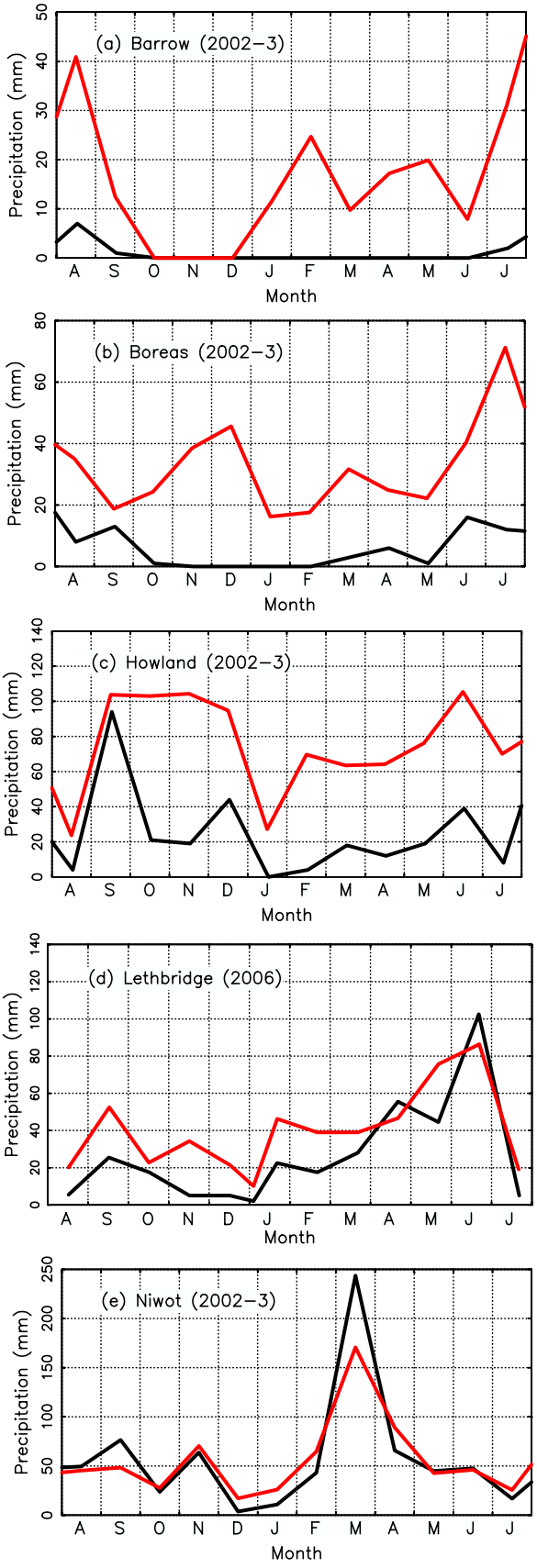

shows a slight positive bias in spring. The Lethbridge site also shows a positive bias, but still falls within observed variability. At the Niwot site, simulated bulk density barely falls within the observed bulk snow densities, which may result from difficulties in specifying the correct snow class. The *Sturm et al.* [1995] snow class map indicates that Niwot is prairie, but since the site is located atop a mountain ridge, we reclassified it as alpine. However, locally observed depth hoar formation indicates that it may be closer to taiga class.

[38] Which snow processes dominate snowpack development varies from site to site and changes during the snow season. At all sites, irregular snow events followed by rapid melting result in high simulated bulk density and shallow snow depth (see Figure 14) in early fall and late spring. At the Barrow and Boreas sites, the snow season starts in September and October, so high simulated density at the start of the snow season does not show up in Figure 8. At Howland, the snow season starts in November, so the simulated snow density starts fairly high, declines as snow accumulates during January and February, and then increases during spring melt in March and April. Frequent snowmelt cycles at Lethbridge result in fairly high simulated density throughout the snow season. Weight compaction is fairly strong at the beginning of the snow season for all sites except Barrow, but slows rapidly when simulated bulk density nears 150–200 kg m^{-3}. Weight compaction is not a dominant factor for the Barrow site because of the development of a relatively incompressible wind slab layer. Thermal aging occurs throughout the snow season at all sites, but is stronger at the beginning and end of the snow season when snow temperatures are higher.

[39] The greatest improvements in simulated bulk snow density occurred at the tundra class site (Barrow) where depth hoar and wind compaction dominate the snowpack development. Prior to introducing the snow class system, the simulated bulk snow density at the Barrow site hovered between 100 and 150 kg m^{-3}, without any noticeable increase during the snow season. Lethbridge, where wind compaction dominates, showed some improvement. The new snow class system only slightly improves simulated bulk snow densities for Howland and Niwot because the original model already included the thermal aging, melting, and weight compaction processes that dominate the maritime and alpine snow classes.

3.3. Soil Organic Matter

[40] The simulated soil organic matter as a function of depth at the Boreas site is consistent in magnitude with observations (Figure 9). The observed soil organic matter shows distinct layering [*Trumbore and Harden*, 1997], while SiBCASA assumes that soil organic matter is proportional to fine root density, resulting in a smooth, exponential decrease with depth. The soil is almost purely organic at the surface and almost pure mineral at 1 m depth. The other sites show a similar level of agreement with available observations of soil organic matter (not shown).

[41] Organic matter strongly influences soil thermodynamic properties, which are determined primarily by soil water

Figure 7. Observed (black) and NARR (red) monthly total precipitation for the winter season of 2002–2003 at all sites except Lethbridge, where we show the monthly precipitation for 2006.

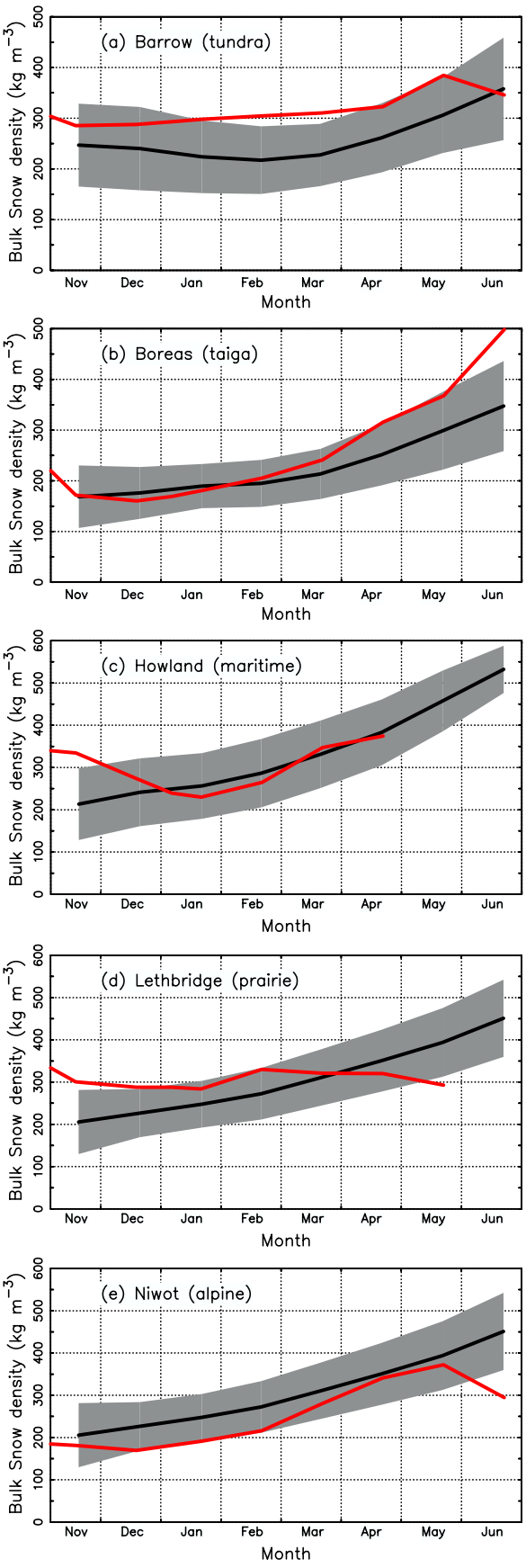

Figure 8. Long-term average of observed bulk snow densities for each snow class (black), standard deviation of observed bulk densities for each class (gray), and simulated bulk densities (red) for each site.

content. Organic soil has higher porosity than pure mineral soil (90 versus ~45%) and much higher hydraulic conductivity (1.0×10^{-4} versus $\sim 2.4 \times 10^{-6}$ m s^{-1}), so organic soil can hold more water, but it drains away quickly. Figure 10 shows how soil organic matter changes the estimated soil thermal conductivity in July 2000 at the Boreas site. In the pure mineral soil, the porosity and hydraulic conductivity are constant with depth, resulting in nearly constant soil water content (~70% saturation) and thermal conductivity with depth. With organic matter, the porosity and hydraulic conductivity are high at the surface and decrease exponentially with depth. The result is well-drained, relatively dry surface soils at ~25% saturation with soil moisture increasing exponentially with depth to ~75% saturation. The slight jump in thermal conductivity at the surface comes from a thin layer of moist soil, a result of a recent rain event. At the Boreas site, the thermal conductivity at the surface is close to that for dry organic soil (0.05 W m^{-1} K^{-1}), a reduction of ~94% compared to pure mineral soil. The soil organic matter decreases and soil moisture content increases with depth such that the thermal conductivity exponentially approaches that for pure mineral soil. The overall result is a thin layer of insulating organic material at the soil surface.

[42] All the sites showed similar vertical profiles in organic matter, porosity, and hydraulic conductivity, but how strongly the surface organic layer insulates the underlying soil depends on the time history of soil moisture content. At the Boreas and Niwot sites, adding soil organic matter allowed the surface soils to dry out in summer, creating an insulating organic soil layer. At Barrow, by contrast, the soils remained nearly saturated all year-round, so adding organic matter did not significantly change the soil thermal conductivity (not shown).

3.4. Soil Temperature

[43] Our changes to the soil and snow models greatly improve the simulation of soil temperatures at Barrow and Boreas, with modest or minimal effect on simulated soil temperatures at the other sites. Figure 11 shows the daily average of observed and simulated soil temperatures, both before and after adding a deeper soil column, the snow classes, and organic soil properties. The time periods shown in Figure 11 differ between sites, depending on the availability of soil temperature data. Howland and Lethbridge show little or no change while Niwot showed modest improvement in simulated summer soil temperatures. The biggest improvement in the simulation of soil temperatures occurred in winter at Barrow and in summer at Boreas.

[44] Warmer than observed simulated soil temperatures in winter produce warmer than observed soil temperatures in summer because of the reemergence effect [*Schaefer et al.*, 2008]. In reemergence, past soil temperature anomalies are stored as variations in the amount of ground ice and can reemerge at the surface after frozen soils thaw in spring. Warm soil temperatures in winter produce shallower winter freeze depths, which require less energy to thaw in spring,

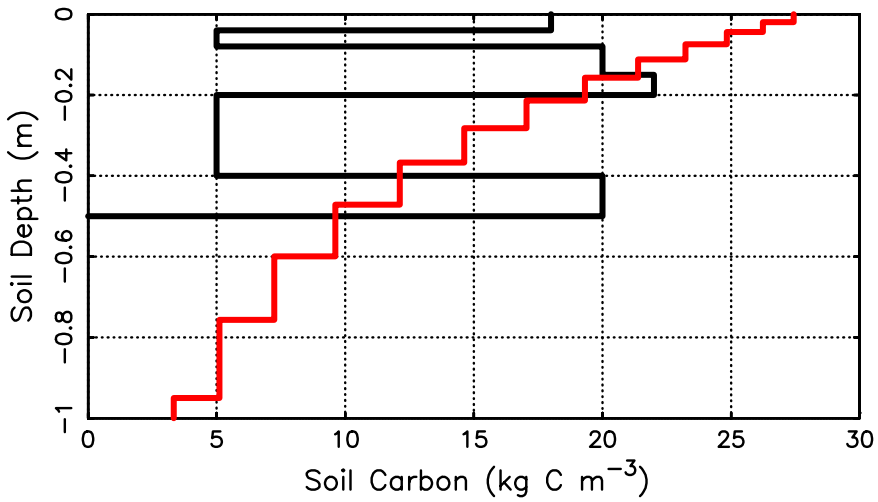

Figure 9. Observed (black) and simulated (red) soil carbon as a function soil depth at the Boreas site.

resulting in warmer simulated soil temperatures the following summer [*Schaefer et al.*, 2008]. Essentially, variations of frozen layer depth modulate summer soil temperatures (except at Barrow, where variations in winter soil temperatures modulate summer active layer depth). The NARR air temperatures match observations well in both magnitude and variability, but even if the NARR temperatures for these sites exactly match observations in spring and summer, deeper snow depths in winter produce warmer than observed soils in summer.

[45] The relative influence of a deeper soil column, snow classes, and organic soil properties on simulated soil temperature differed between Barrow and Boreas. To correctly simulate the flow of energy between the atmosphere and the soil, and thus soil temperatures, both the snowpack and soil must have the correct thermal properties. At Barrow, the original model had difficulty simulating realistic snow density and associated thermal conductivity, so the new snow classes produced the biggest change in simulated soil temperatures. At Boreas, the soil thermal conductivity was too high, so the new organic soil properties produced the biggest change in simulated soil temperature. Figures 12 and 13 illustrate how the relative influence of each change differs between sites by comparing observed soil temperatures as a function of depth to simulated temperatures with the original version of SiBCASA, SiBCASA with all the modifications, and SiBCASA with each of the changes acting alone. Figures 12 and 13 cover the same time periods for Barrow and Boreas as shown in Figure 11.

[46] At Barrow, observations indicate cold soils in winter with a summer active layer depth of about 40–50 cm (Figure 12a). In the original model, the entire 3.4 m soil column thawed each summer and froze each winter, with annual average temperatures of ~0°C (Figure 12c). Making the soil column deeper increased the total soil heat capacity and stabilized the active layer depth to 1.2 m, but annual average soil temperatures still hovered just below freezing (Figure 12e). Adding only the organic soil properties had almost no effect on simulated soil temperatures (Figure 12f) because the soils generally stayed saturated through summer. Because the snow density was so low in the original model, adding only the effects of wind slab and depth hoar snow

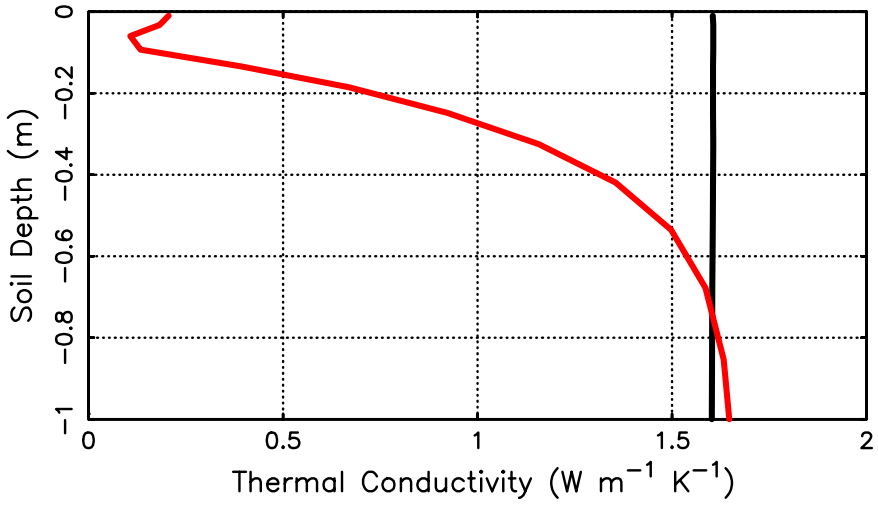

Figure 10. Simulated soil thermal conductivity as a function of depth for pure mineral soil (black) and accounting for soil organic matter (red) at the Boreas site in July 2000.

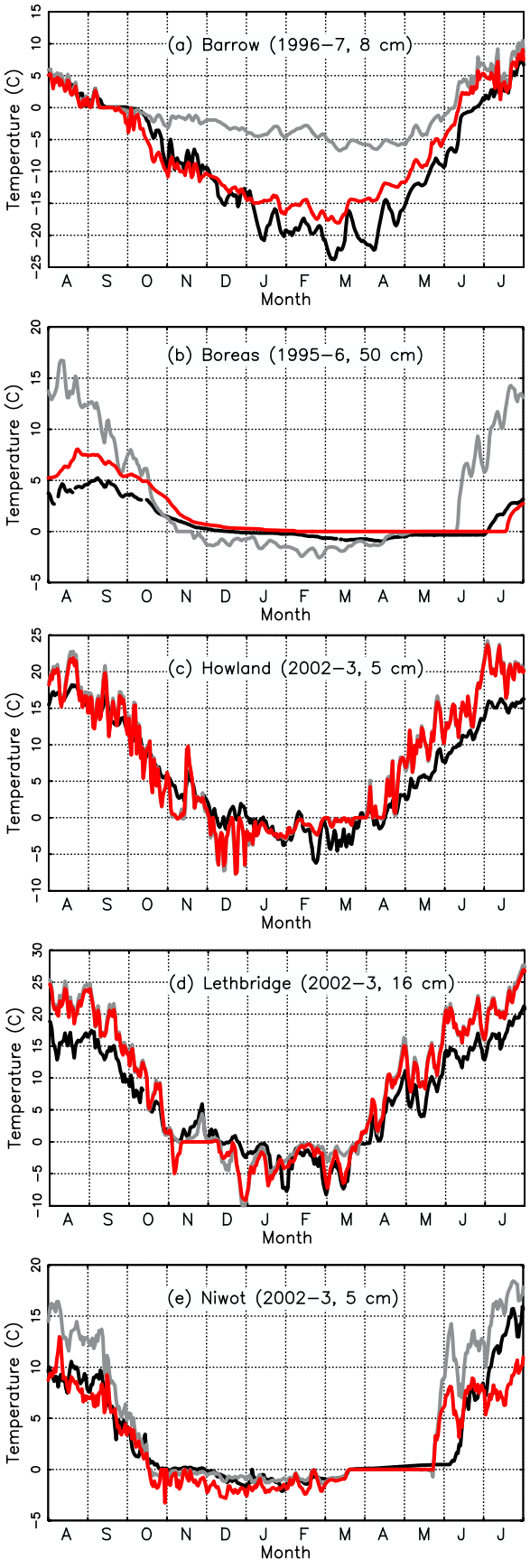

Figure 11. Daily average soil temperatures for the winter season at each site, showing observed values (black); simulated values using original model (gray); and simulated values with a deeper soil column, snow classes, and organic soil properties (red). The time period and depth of observations appear in parentheses.

associated with the new snow classes had the biggest influence on simulated soil temperatures, although the entire soil column still thawed each summer (Figure 12d).

[47] Although the new snow classes produced the biggest changes at Barrow, only the combined effects of all three changes produced realistic soil temperatures and freeze/thaw dynamics (Figure 12b). The snow classes increase the snow thermal conductivity, decreasing winter soil temperatures. The high porosity of organic soil properties increases the soil moisture content and the heat capacity of the soil, reducing the simulated active layer depth. The increased heat capacity of a deeper soil column stabilizes the active layer depth. The result is significantly colder soils in winter and simulated active layer depths of ~70 cm (observed active layer depths vary between of 40 and 50 cm [*Zhang et al.*, 1996]). The changes compliment and amplify each other to produce larger improvements in simulated soil temperatures than each change acting alone.

[48] At Boreas, observations indicate a winter freeze depth in excess of 1m with warm surface soils and relatively cool deep soils in summer (Figure 13a). The original model produced realistic winter freeze depths, but the summer soil temperatures were too high and extended far too deep into the soil column (Figure 13c). A deeper soil column or snow classes did not significantly change the simulated summer soil temperatures (Figures 13d and 13e). The warm simulated summer soil temperatures indicated the original soil thermal conductivity was too high, so decreased thermal conductivity associated with the new organic soil properties strongly influenced simulated soil temperatures (Figure 13f). Although the amplification effect is not nearly so pronounced as at Barrow, the combined effects of all three changes produce the best overall results (Figure 13b).

3.5. Snow Depth

[49] Differences between simulated and observed soil temperatures result in part from differences between simulated and observed snow depth and associated insulation effects. Figure 14 shows simulated and observed snow depths from the nearest National Weather Service cooperative observing station. Simulated snow depth at the Barrow site is slightly higher than observed; simulated snow depths at the Howland and Niwot sites match observed values reasonably well; and the Boreas and Lethbridge sites show large mismatches. The deeper than observed snow at the Boreas site increases the insulation effect, resulting in warmer than observed soil temperatures. At Lethbridge, simulated and observed D match well in the early part of the winter season, but not the later part, resulting in slightly colder than observed soil temperatures in early winter and warmer than observed in late winter.

[50] Some of the differences between simulated and observed snow depth result from using NARR meteorology as input. At the Barrow and Boreas sites, NARR precipitation is nearly double observed, and with such long winters, most

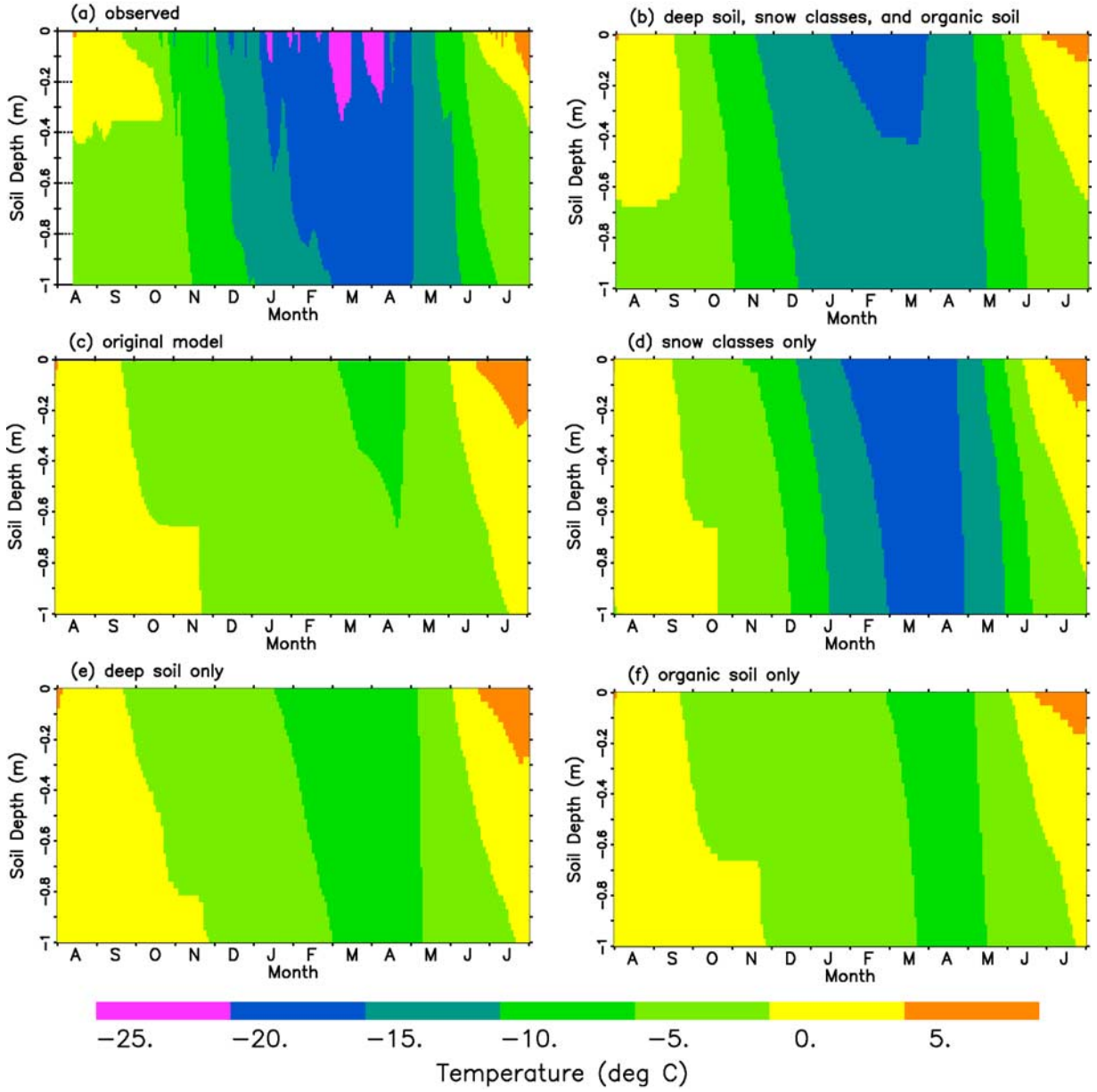

Figure 12. Daily average soil temperature as a function of depth at Barrow for the winter of 1996–1997. (a) Observed; (b) simulated with deeper soil column, snow classes, and organic soil properties; (c) simulated with original model; (d) simulated with snow classes only; (e) simulated with deeper soil column only; and (f) simulated with organic soil properties only.

of this excess precipitation falls as snow, resulting in larger snow depth than observed. At Howland, the annual NARR precipitation is more than double the observed precipitation. The apparent match with observations may result from the fact that the observed values come from a station 40 km away. At the Lethbridge site, the NARR winter precipitation is higher than observed, which can partially explain the deeper than observed snow. The observed air temperatures at Lethbridge in winter hover near freezing and the −3°C NARR temperature bias is sufficient to greatly reduce melting, amplifying the snow depth bias due to excessive NARR precipitation. NARR and observed precipitation match quite well at Niwot, with a corresponding match in snow depth and soil temperature.

[51] Errors in simulated snow depth can change simulated soil temperatures by several degrees. In several model experiments at Barrow and Boreas, we scaled down the NARR precipitation for a specific season or for the entire time series to match local observations of snow depth. Scaling down NARR precipitation at Barrow and Boreas to improve simulated snow depth reduced the insulating effect of the snow, decreasing simulated soil temperature in both winter and summer by 1° to 3°C (not shown).

4. Discussion and Conclusions

[52] Adding the effects of depth hoar and wind slab development on snow density, the effects of organic matter on soil

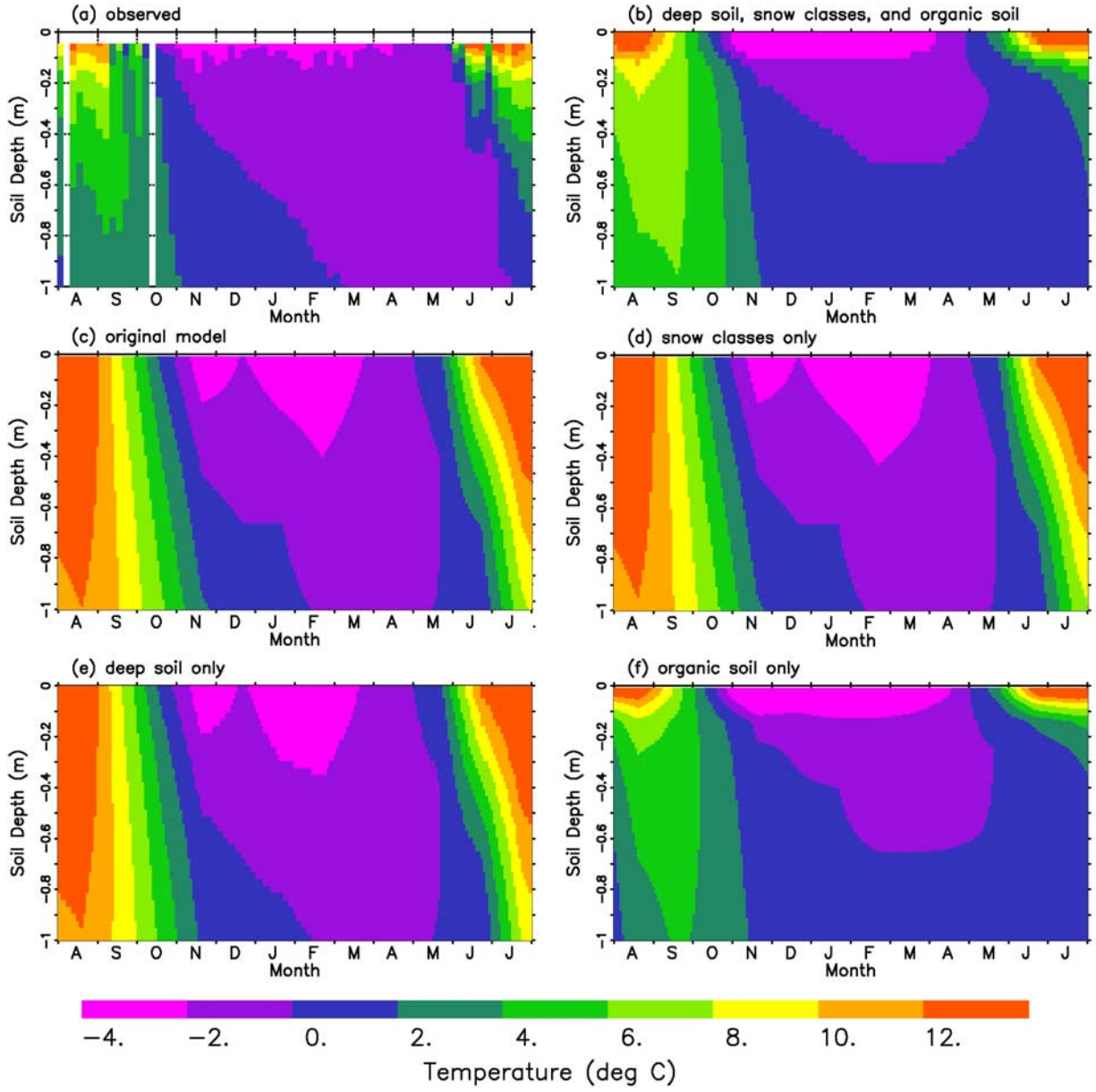

Figure 13. Daily average soil temperature as a function of depth at Boreas for the winter of 1995–1996. (a) Observed; (b) simulated with deeper soil column, snow classes, and organic soil properties; (c) simulated with original model; (d) simulated with snow classes only; (e) simulated with deeper soil column only; and (f) simulated with organic soil properties only.

properties, and a deeper soil column improved simulated soil temperatures and freeze/thaw dynamics at high latitudes in SiBCASA. The greatest improvement in simulated bulk snow density, snow depth, and soil temperature occurred at the tundra site (Barrow) and the taiga site (Boreas), where depth hoar and wind compaction dominate the snowpack development. Adding snow classes had the biggest effect on simulated soil temperature at Barrow and adding organic soil properties had the biggest effect at Boreas. The SiBCASA soil and snow models already included the locally dominant snow and soil processes at the midlatitude maritime, prairie, and alpine sites (Howland, Lethbridge, and Niwot), so the deeper soil column, snow classes, and organic soil properties resulted in only modest improvements in simulated soil temperature. We found this quite encouraging because SiBCASA already predicted fairly realistic soil temperatures at midlatitude sites and our changes were specifically targeted to improve the simulation of permafrost.

[53] Differences between NARR and observed weather influenced the simulated soil temperatures. The NARR air temperature captured the seasonal and synoptic variability of the observed air temperature. However, the simulated soil temperatures did reflect small seasonal biases between NARR and observed air temperature. At all sites except Niwot, the NARR precipitation was greater than observed, resulting in deeper than observed snow. This strengthened the insulating effect of the snowpack, resulting in warmer than observed soil temperatures. At all sites, differences between simulated

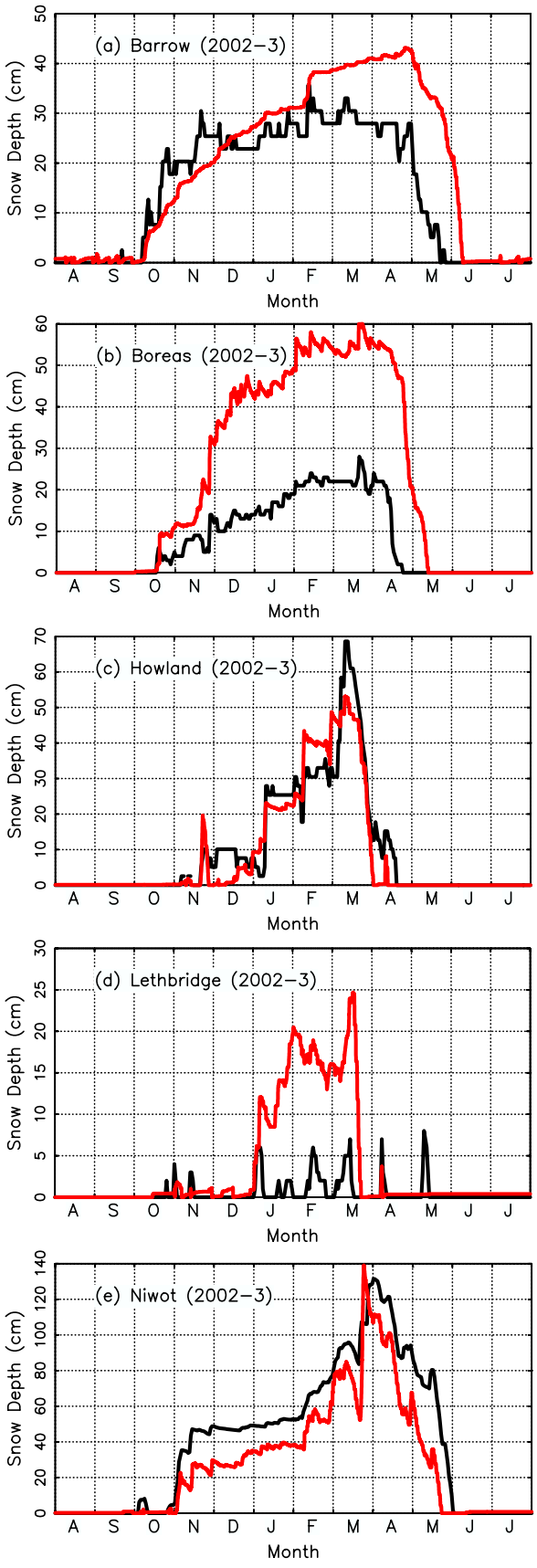

Figure 14. Observed snow depths from nearest cooperative observing station (black) and simulated snow depth (red) for the winter season of 2002–2003 at each site.

and observed soil temperatures in winter resulted in differences in summer, due to the reemergence effect.

[54] Using a snow classification system incorporates the effects of depth hoar development and wind compaction without explicitly modeling these processes. The depth hoar thermal conductivities and wind speed-dependent snowfall density represent highly simplified, but effective representations of depth hoar development and wind compaction. The changes we describe could improve the representation of high-latitude snow and soil freeze/thaw processes in many LSMs with minimal additional complexity and computational cost.

[55] As we hypothesized, only the combined effects of snow classes, organic soil properties, and a deeper soil column significantly improved simulated soil temperatures and freeze/thaw dynamics at high latitudes. How well a model simulates soil temperature depends on how well it represents the actual flow of energy between the atmosphere and the soil, which depends on the simulated thermal properties of both snow and soil. In our simulations, changing snow conductivity without changing soil conductivity (or vice versa) did not significantly alter the flow of energy between the atmosphere and the ground to improve simulated soil temperatures and freeze/thaw dynamics. Only the combined effects of the increased thermal inertia of the deeper soil column, the improved representation of depth hoar and wind slab layers in the snow classes, and the decreased thermal conductivity of organic matter produced the correct energy flow, and thus soil temperatures.

[56] Our results represent an example of "process interdependency" in model development, where only the combined effects of multiple changes in several submodels can achieve the desired result, while the individual changes, taken separately, do not. LSMs today contain all the primary physical and biological processes, but as we push our models to more extreme applications, we have to add multiple, interconnected secondary processes to improve results. To improve simulated soil temperatures and freeze/thaw dynamics at high latitudes in SiBCASA, we had to simultaneously change both the snow and soil submodels. We added the effects of depth hoar and wind compaction to the snow model and the effects of organic matter and a deeper soil column to the soil model. Taken separately, these changes had minimal or modest effect, but in combination, these changes greatly improved simulated soil temperatures and freeze/thaw dynamics at high latitudes.

[57] **Acknowledgments.** This study was in part supported by the U.S. National Aeronautics and Space Administration (NASA) grant NNX06AE65G, the U.S. National Oceanic and Atmospheric Administration (NOAA) grant NA07OAR4310115, and the U.S. National Science Foundation (NSF) grant OPP-0352957 to the University of Colorado at Boulder.

References

Alexeev, V. A., D. J. Nicolsky, V. E. Romanovsky, and D. M. Lawrence (2007), An evaluation of deep soil configurations in the CLM3 for improved representation of permafrost, *Geophys. Res. Lett.*, *34*, L09502, doi:10.1029/2007GL029536.

Anderson, E. A. (1976), A point energy and mass balance model of a snow cover, *Tech. Rep. 19*, NOAA, Washington, D. C.

Baldocchi, D. D. (2003), Assessing the eddy covariance technique for evaluating carbon dioxide exchange rates of ecosystems: Past, present and future, *Global Change Biol.*, *9*(4), 479–492, doi:10.1046/j.1365-2486.2003.00629.x.

Ball, J. T. (1988), An analysis of stomatal conductance, Ph.D. thesis, Stanford Univ., Stanford, Calif.

Berner, J., et al. (2005), *Arctic Climate Impact Assessment*, edited by C. Symon, L. Arris, and B. Heal, 1042 pp., Cambridge Univ. Press, Cambridge, U. K.

Bonan, G. B. (1996), A Land Surface Model (LSM Version 1.0) for ecological, hydrological, and atmospheric studies: Technical description and users guide, *Tech. Note NCAR/TN-417+STR*, Natl. Cent. for Atmos. Res., Boulder Colo.

Brown, J., K. M. Hinkel, and F. E. Nelson (2000), The Circumpolar Active Layer Monitoring (CALM) program: Research designs and initial results, *Polar Geogr.*, *24*(3), 165–258, doi:10.1080/10889370009377697.

Brown, R. D. (2000), Northern Hemisphere snow cover variability and change, 1915–97, *J. Clim.*, *13*(13), 2339–2355, doi:10.1175/1520-0442(2000)013<2339:NHSCVA>2.0.CO;2.

Collatz, G. J., J. T. Ball, C. Grivet, and J. A. Berry (1991), Physiological and environmental regulation of stomatal conductance, photosynthesis, and transpiration: A model that includes a laminar boundary layer, *Argic. For. Meteorol.*, *54*, 107–136, doi:10.1016/0168-1923(91)90002-8.

Collatz, G. J., M. Ribascarbo, and J. A. Berry (1992), Coupled photosynthesis-stomatal conductance model for leaves of C4 plants, *Aust. J. Plant Physiol.*, *19*(5), 519–538.

Dai, Y., et al. (2003), The common land model, *Bull. Am. Meteorol. Soc.*, *84*(8), 1013–1023, doi:10.1175/BAMS-84-8-1013.

Delisle, G. (2007), Near-surface permafrost degradation: How severe during the 21st century?, *Geophys. Res. Lett.*, *34*, L09503, doi:10.1029/2007GL029323.

Denning, A. S., G. J. Collatz, C. Zhang, D. A. Randall, J. A. Berry, P. J. Sellers, G. D. Colello, and D. A. Dazlich (1996), Simulations of terrestrial carbon metabolism and atmospheric CO_2 in a general circulation model. Part 1: Surface carbon fluxes, *Tellus*, *48*, 521–542, doi:10.1034/j.1600-0889.1996.t01-2-00009.x.

Domine, F., A. Cabanes, and L. Legagneux (2002), Structure, microphysics, and surface area of the Arctic snowpack near Alert during the ALERT 2000 campaign, *Atmos. Environ.*, *36*(15–16), 2753–2765, doi:10.1016/S1352-2310(02)00108-5.

Dunn, A. L., C. C. Barford, S. C. Wofsy, M. L. Goulden, and B. C. Daube (2007), A long-term record of carbon exchange in a boreal black spruce forest: Means, responses to interannual variability, and decadal trends, *Global Change Biol.*, *13*(3), 577–590, doi:10.1111/j.1365-2486.2006.01221.x.

Eugster, W., et al. (2000), Land-atmosphere energy exchange in Arctic tundra and boreal forest: Available data and feedbacks to climate, *Global Change Biol.*, *6*, 84–115, doi:10.1046/j.1365-2486.2000.06015.x.

Farquhar, G. D., S. von Caemmerer, and J. A. Berry (1980), A biochemical model of photosynthetic CO_2 assimilation in leaves of C3 species, *Planta*, *149*, 78–90, doi:10.1007/BF00386231.

Frauenfeld, O., T. Zhang, R. G. Barry, and D. G. Gilichinsky (2004), Interdecadal changes in seasonal freeze and thaw depths in Russia, *J. Geophys. Res.*, *109*, D05101, doi:10.1029/2003JD004245.

Fuchs, M., G. S. Campbell, and R. I. Papendick (1978), Analysis of sensible and latent heat-flow in a partially frozen unsaturated soil, *Soil Sci. Soc. Am. J.*, *42*(3), 379–385.

Hinkel, K. M. (1998), Soil Temperatures for Happy Valley and Barrow, Alaska, USA, http://nsidc.org/data/arcss038.html, Natl. Snow and Ice Data Cent., Boulder, Colo., (Updated in 2004.).

Hollinger, D. Y., et al. (2004), Spatial and temporal variability in forest-atmosphere CO_2 exchange, *Global Change Biol.*, *10*(11), 1689–1706, doi:10.1111/j.1365-2486.2004.00892.x.

Iida, T., K. Ueki, H. Tsukahara, and A. Kajihara (2000), Point physical model of movement of ions through natural snow cover, *J. Hydrol.*, *235*(3–4), 170–182, doi:10.1016/S0022-1694(00)00257-2.

Intergovernmental Panel on Climate Change (2007), *Climate Change 2007: Synthesis Report. Contribution of Working Groups I, II and III to the Fourth Assessment Report of the Intergovernmental Panel on Climate Change*, edited by R. K. Pachauri and A. Reisinger, 104 pp., Geneva, Switzerland.

Jenkins, J. C., R. A. Birdsey, and Y. Pan (2001), Biomass and NPP estimation for the mid-Atlantic region (USA) using plot-level forest inventory data, *Ecol. Appl.*, *11*(4), 1174–1193, doi:10.1890/1051-0761(2001)011[1174:BANEFT]2.0.CO;2.

Jorgenson, M. T., C. H. Racine, J. C. Walters, and T. E. Osterkamp (2001), Permafrost degradation and ecological changes associated with a warming climate in central Alaska, *Clim. Change*, *48*(4), 551–579, doi:10.1023/A:1005667424292.

Judson, A., and N. Doesken (2000), Density of freshly fallen snow in the central Rocky Mountains, *Bull. Am. Meteorol. Soc.*, *81*(7), 1577–1587, doi:10.1175/1520-0477(2000)081<1577:DOFFSI>2.3.CO;2.

Lawrence, D. M., and A. G. Slater (2008), Incorporating organic soil into a global climate model, *Clim. Dyn.*, *30*(2–3), 145–160.

Lawrence, D. M., A. G. Slater, V. E. Romanovsky, and D. J. Nicolsky (2008), Sensitivity of a model projection of near-surface permafrost degradation to soil column depth and representation of soil organic matter, *J. Geophys. Res.*, *113*, F02011, doi:10.1029/2007JF000883.

Ling, F., and T. Zhang (2004), A numerical model for surface energy balance and thermal regime of the active layer and permafrost containing unfrozen water, *Cold Reg. Sci. Technol.*, *38*, 1–15, doi:10.1016/S0165-232X(03)00057-0.

Ling, F., and T. Zhang (2005), Modeling the effect of variations in snowpack-disappearance date on surface-energy balance on the Alaskan North Slope, *Arct. Antarct. Alp. Res.*, *37*(4), 483–489, doi:10.1657/1523-0430(2005)037[0483:MTEOVI]2.0.CO;2.

Liston, G. E., and M. Sturm (1998), Global Seasonal Snow Classification System, http://nsidc.org/data/arcss045.html, Natl. Snow and Ice Data Cent., Boulder, Colo.

Los, S. O., G. J. Collatz, L. Bounoua, P. J. Sellers, and C. J. Tucker (2001), Global interannual variations in sea surface temperature and land-surface vegetation, air temperature, and precipitation, *J. Clim.*, *14*(7), 1535–1549, doi:10.1175/1520-0442(2001)014<1535:GIVISS>2.0.CO;2.

Mesinger, F., et al. (2006), North American Regional Reanalysis, *Bull. Am. Meteorol. Soc.*, *87*(3), 343–360, doi:10.1175/BAMS-87-3-343.

Miller, S. D., M. L. Goulden, M. C. Menton, H. R. da Rocha, H. C. de Freitas, A. Figueira, and C. de Sousa (2004), Biometric and micrometeorological measurements of tropical forest carbon balance, *Ecol. Appl.*, *14*(4), 114–126, doi:10.1890/02-6005.

Monson, R. K., A. A. Turnipseed, J. P. Sparks, P. C. Harley, L. E. Scott-Denton, K. Sparks, and T. E. Huxman (2002), Carbon sequestration in a high-elevation, subalpine forest, *Global Change Biol.*, *8*(5), 459–478, doi:10.1046/j.1365-2486.2002.00480.x.

Natural Resources Conservation Service (2007), Snow Course Data, http://www.wcc.nrcs.usda.gov/snowcourse/snow_rpt.html, Washington, D. C.

Nicolsky, D. J., V. E. Romanovsky, V. A. Alexeev, and D. M. Lawrence (2007), Improved modeling of permafrost dynamics in a GCM land-surface scheme, *Geophys. Res. Lett.*, *34*, L08501, doi:10.1029/2007GL029525.

Oleson, K. W., W. J. Emery, and J. A. Maslanik (2000), Evaluating land surface parameters in the Biosphere-Atmosphere Transfer Scheme using remotely sensed data sets, *J. Geophys. Res.*, *105*(D6), 7275–7293, doi:10.1029/1999JD901041.

Osterkamp, T. E. (2007), Characteristics of the recent warming of permafrost in Alaska, *J. Geophys. Res.*, *112*, F02S02, doi:10.1029/2006JF000578.

Peters-Lidard, C. D., E. Blackburm, X. Liang, and E. F. Wood (1998), The effect of soil thermal conductivity parameterization on surface energy fluxes and temperatures, *J. Atmos. Sci.*, *55*, 1209–1224, doi:10.1175/1520-0469(1998)055<1209:TEOSTC>2.0.CO;2.

Price, J. S., J. Cagampan, and E. Kellner (2005), Assessment of peat compressibility: Is there an easy way?, *Hydrol. Processes*, *19*(17), 3469–3475, doi:10.1002/hyp.6068.

Sato, T., K. Kosugi, S. Mochizuki, and M. Nernoto (2008), Wind speed dependences of fracture and accumulation of snowflakes on snow surface, *Cold Reg. Sci. Technol.*, *51*(2–3), 229–239, doi:10.1016/j.coldregions.2007.05.004.

Schaefer, K., A. S. Denning, N. Suits, J. Kaduk, I. Baker, S. Los, and L. Prihodko (2002), Effect of climate on interannual variability of terrestrial CO_2 fluxes, *Global Biogeochem. Cycles*, *16*(4), 1102, doi:10.1029/2002GB001928.

Schaefer, K., A. S. Denning, and O. Leonard (2005), The winter Arctic Oscillation, the timing of spring, and carbon fluxes in the Northern Hemisphere, *Global Biogeochem. Cycles*, *19*, GB3017, doi:10.1029/2004GB002336.

Schaefer, K., T. Zhang, P. Tans, and R. Stöckli (2007), Temperature anomaly reemergence in seasonally frozen soils, *J. Geophys. Res.*, *112*, D20102, doi:10.1029/2007JD008630.

Schaefer, K., G. J. Collatz, P. Tans, A. S. Denning, I. Baker, J. Berry, L. Prihodko, N. Suits, and A. Philpott (2008), Combined Simple Biosphere/Carnegie-Ames-Stanford Approach terrestrial carbon cycle model, *J. Geophys. Res.*, *113*, G03034, doi:10.1029/2007JG000603.

Sellers, P. J., Y. Mintz, Y. C. Sud, and A. Dalcher (1986), A Simple Biosphere Model (SiB) for use within general circulation models, *J. Atmos. Sci.*, *43*(6), 505–531, doi:10.1175/1520-0469(1986)043<0505:ASBMFU>2.0.CO;2.

Sellers, P. J., C. J. Tucker, G. J. Collatz, S. O. Los, C. O. Justice, D. A. Dazlich, and D. A. Randall (1994), A global 1° by 1° NDVI data set for climate studies. Part 2: The generation of global fields of terrestrial biophysical parameters from NDVI, *Int. J. Remote Sens.*, *15*(17), 3519–3545, doi:10.1080/01431169408954343.

Sellers, P. J., D. A. Randall, G. J. Collatz, J. A. Berry, C. B. Field, D. A. Dazlich, C. Zhang, G. D. Collelo, and L. Bounoua (1996a), A revised land surface parameterization of GCMs. Part I: Model formulation, *J. Clim.*, *9*(4), 676–705, doi:10.1175/1520-0442(1996)009<0676:ARLSPF>2.0.CO;2.

Sellers, P. J., C. J. Tucker, G. J. Collatz, S. O. Los, C. O. Justice, D. A. Dazlich, and D. A. Randall (1996b), A revised land surface parameterization of GCMs. Part II: The generation of global fields of terrestrial biophysical parameters from satellite data, *J. Clim.*, *9*(4), 706–737, doi:10.1175/1520-0442(1996)009<0706:ARLSPF>2.0.CO;2.

Stroeve, J., M. M. Holland, W. Meier, T. Scambos, and M. Serreze (2007), Arctic sea ice decline: Faster than forecast, *Geophys. Res. Lett.*, *34*, L09501, doi:10.1029/2007GL029703.

Sturm, M., J. Holgrem, and G. E. Liston (1995), A seasonal snow cover classification system for local to global applications, *J. Clim.*, *8*(5), 1261–1283, doi:10.1175/1520-0442(1995)008<1261:ASSCCS>2.0.CO;2.

Sturm, M., J. Holmgren, M. Konig, and K. Morris (1997), The thermal conductivity of seasonal snow, *J. Glaciol.*, *43*(143), 26–41.

Sturm, M., C. Derksen, G. Liston, A. Silis, D. Solie, J. Holmgren, and H. Huntington (2008), A reconnaissance snow survey across Northwest territories and Nunavut, Canada, April 2007, *Tech. Rep. ERDC/CRREL TR-08-3*, Eng. Res. and Dev. Cent., Hanover, N. H.

Su, Z., and Y. E. Shi (2002), Response of monsoonal temperate glaciers to global warming since the Little Ice Age, *Quat. Int.*, *97–98*, 123–131, doi:10.1016/S1040-6182(02)00057-5.

Sutton, D., M. L. Goulden, A. Bazzaz, B. C. Daube, S.-M. Fan, J. W. Munger, and S. Wofsy (1998), BOREAS TF-03 NSA-OBS Tower Flux, Meteorological, and Soil Temperature Data, http://daac.ornl.gov/BOREAS/guides/TF03_Flux_Met.html, Oak Ridge Natl. Lab. Distrib. Active Arch. Cent., Oak Ridge, Tenn.

Trumbore, S. E., and J. W. Harden (1997), Accumulation and turnover of carbon in organic and mineral soils of the BOREAS northern study area, *J. Geophys. Res.*, *102*(D24), 28,817–28,830, doi:10.1029/97JD02231.

Tucker, C. J., J. E. Pinzon, M. E. Brown, D. A. Slayback, E. W. Pak, R. Mahoney, E. F. Vermote, and N. El Saleous (2005), An extended AVHRR 8-km NDVI dataset compatible with MODIS and SPOT vegetation NDVI data, *Int. J. Remote Sens.*, *26*(20), 4485–4498, doi:10.1080/01431160500168686.

Vidale, P. L., and R. Stöckli (2005), Prognostic canopy air space solutions for land surface exchanges, *Theor. Appl. Climatol.*, *80*, 245–257, doi:10.1007/s00704-004-0103-2.

Williams, P. J., and M. W. Smith (1989), *The Frozen Earth: Fundamentals of Geocryology*, 304 pp., Cambridge Univ. Press, Cambridge, U. K.

Yao, T., J. Pu, A. Lu, Y. Wang, and W. Yu (2007), Recent glacial retreat and its impact on hydrological processes on the tibetan plateau, China, and sorrounding regions, *Arct. Antarct. Alp. Res.*, *39*(4), 642–650, doi:10.1657/1523-0430(07-510)[YAO]2.0.CO;2.

Yi, S. H., M. K. Woo, and M. A. Arain (2007), Impacts of peat and vegetation on permafrost degradation under climate warming, *Geophys. Res. Lett.*, *34*, L16504, doi:10.1029/2007GL030550.

Zhang, T. (2005), Influence of the seasonal snow cover on the ground thermal regime: An overview, *Rev. Geophys.*, *43*, RG4002, doi:10.1029/2004RG000157.

Zhang, T., T. E. Osterkamp, and K. Stamnes (1996), Some characteristics of the climate in Northern Alaska, U.S.A., *Arct. Antarct. Alp. Res.*, *28*(4), 509–518.

Zhang, T. J., et al. (2005), Spatial and temporal variability in active layer thickness over the Russian Arctic drainage basin, *J. Geophys. Res.*, *110*, D16101, doi:10.1029/2004JD005642.

Zhang, Y., W. J. Chen, and D. W. Riseborough (2008), Disequilibrium response of permafrost thaw to climate warming in Canada over 1850–2100, *Geophys. Res. Lett.*, *35*, L02502, doi:10.1029/2007GL032117.

I. Baker and L. Lu, Department of Atmospheric Science, Colorado State University, Fort Collins, CO 80523-1371, USA.

A. Etringer, K. Schaefer, A. G. Slater, and T. Zhang, National Snow and Ice Data Center, Cooperative Institute for Research in Environmental Sciences, University of Colorado at Boulder, 449 UCB, Boulder, CO 80309-0449, USA. (kevin.schaefer@nsidc.org)